# Visualizing Acoustic Imaging of Hydrothermal Plumes on the Seafloor

[1]Li Liu, [2]Deborah Silver, [3]Karen Bemis

1. School of Computer Science and Technology, Soochow University, Suzhou, China.
2. Department of Electrical and Computer Engineering, Rutgers, The State University of New Jersey, New Brunswick, NJ 08901, USA.
3. Department of Marine and Coastal Sciences, Rutgers, The State University of New Jersey, New Brunswick, NJ 08901, USA.

## Abstract

Hydrothermal plumes are ongoing venting of hot solutions, on a time scale of months to years, relating to volcanic activities on the seafloor. Recent developments in acoustical observational techniques has produced images to support the scientific investigation of such plumes. However, understanding the complex behavior of plumes in a long-time series poses a challenge to the existing analysis approaches. The motivation of this work is to use visualization techniques to facilitate the visual exploration and analysis of plumes and to help domain scientists compare the actual behavior of plumes predicted by tidal interaction models and buoyant plume models incorporating forced entrainment effects. Methods of geovisualization are combined with time-varying feature-based techniques to create visualizations of plumes which are applied to an acoustic imaging data collected from the Cabled Observatory Vent Imaging System in the Northeast Pacific. The results give new insights to the data and confirm the hypothesis of plumes.

**Keywords:** 3D geovisualization, WebGL, time-varying data, acoustic imaging, hydrothermal plume, feature tracking

## 1. Introduction

Hydrothermal plumes are hot fluids rising from hot springs found along mid-ocean ridges and atop volcanically-active seamounts, where the supply of hot fluids is driven by magmatic heat sources [1]. Such plumes act as agents of dispersal of heat and chemicals transferred from the lithosphere into the ocean supporting ecosystems, changing ocean chemistry, and affecting ocean circulation [2]. A hydrothermal plume is characterized by rapid discharge of high-temperature (>250°C) fluid through particle-rich sulfide chimneys, followed by rising through the surrounding water. As the plumes rise, they entrain, or incorporate, water from their surroundings resulting expansion; they rise until the plume density matches that of the surrounding water, at which point the plume begins to expand laterally [3]. The interaction of hydrothermal plumes with the ocean is studied in order to further scientific understanding of how the dispersal of the heat and chemicals carried by these plumes may be affected by different types of ocean currents and geologic events [4].

Tidal forces, generated by gravitational interactions between astronomical bodies, drive the most common ocean currents, which are often described as sloshing back-and-forth. However, ideal tidally-driven currents describe a circular motion at the ocean surface which flattens to elliptical motion internally and linear motion at the seafloor; actual tidal currents are additionally distorted due to the effects of the Earth's rotation and seafloor geometry. In addition, a variety of processes, including atmospheric storms and tsunamis, can drive internal currents in the ocean; these non-tidal currents may or may not be periodic. Studies of ocean currents at mid-oceanic ridges find currents with tidal, inertial, and weather-band periodicities as well as aperiodic currents related to large scale entrainment by hydrothermal plumes and other processes [5]. Both tidal and non-tidal currents affect plumes by bending the plumes in the direction of transport, increasing the entrainment of the surrounding water into the plume, and changing the dominate direction of transport of heat and chemicals. Basin-scale ocean circulation currents can result in the transport of hydrothermal fluids across an ocean basin [2].

Over the last two decades, two- and three-dimensional plume images have been produced by the joint development of visualization and acoustic methods, which supports the scientific investigation and monitoring of hydrothermal plumes and other hydrothermal flow regimes. However, the existing methods tend to focus on a single data frame or use 2D plots to analyze the motion and physical properties of plumes. In studying the behaviors and characteristics of hydrothermal plumes, oceanographers always want to ask: "What is the general pattern of plume bending? Does the leaning vary systematically in time? How do different plumes interact with each other?" Answering these questions requires understanding and quantifying the complex temporal behavior of plumes in long time-series, which poses a challenge to the existing approaches. Sometimes, scientists illustrate their hypotheses about these questions as idealized cartoons such as the example shown in Figure 1. The creation of these illustrations involves manual inspection of all timesteps of a dataset to pick out representative timesteps (key frames) and constructing a composite image or sequence of images to illustrate the idea or hypothesis. While resulting in effective illustrations, these approaches depend critically on a domain expert's

This article has been accepted for publication in a future issue of this journal, but has not been fully edited. Content may change prior to final publication. Citation information: DOI 10.1109/MCG.2020.2995077, IEEE Computer Graphics and Applications

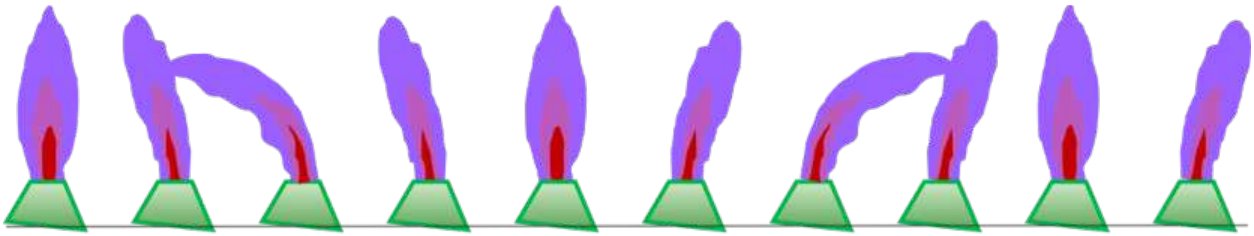

Figure 1. Artistic illustration of hydrothermal plume drawn by ocean scientists. The cartoon diagram shows five idealized phases of plume bending (i.e., big left, small left, vertical, small right, and big right) in respond to tidal currents.

unquantified judgement and can easily miss some instances of events in long time series.

The goal of this paper is to automatically create a set of visualizations from acoustic imaging of hydrothermal plumes to facilitate the visual exploration and quantitative analysis of the data and thus to help domain scientists compare the actual behavior of plumes predicted by tidal interaction models and buoyant plume models incorporating forced entrainment effects. The data used in this work is acoustic imaging of hydrothermal plumes collected from the Cabled Observatory Vent Imaging System (COVIS) in the Northeast Pacific.

Visualizing geospatial data plays an important role in analyzing and understanding geographic phenomena in earth science and related disciplines [6]. A number of techniques and methods adapted from the fields such as cartography and scientific visualization are studied and applied in geospatial data and these techniques are accumulated to what known as geovisualization [7]. This work combines the methods of geovisualization with time-varying feature-based techniques (e.g., feature tracking) to create four types of visualizations to tell a full visual story of plumes rising from hydrothermal vents by giving different insights of the acoustic imaging data and elucidating the linkages of the elliptical plume motion with oceanic and geological external forcing fields. Several visual effectiveness enhancement techniques along with careful color-coding schemes are applied to the proposed visualizations to give sufficient artistic freedom to depict the elliptical plume motion in an expressive way. A WebGL-based viewer is developed to present the visualizations of plume on any web browsers.

## 2. Related Work

Previous research related to the methodologies adopted in this paper includes time-varying volume visualizations and the visualization of geospatial data.

Time-varying volume visualizations usually fall into two major categories: time-independent algorithms and time-dependent algorithms. Time-independent algorithms process multiple timesteps independently and display the sequence of timesteps as an animation. Related methods generally include reducing the storage size of data to make the data more manageable (e.g., temporal subsampling, compression, and contouring), preselecting transfer functions for direct volume rendering, and interactive hardware-accelerated volume rendering [8]. In contrast, time-dependent algorithms introduce a dependency between neighboring timesteps. Two common methods are particle tracing and feature extraction and tracking (also known as feature-based method). Particle tracing is a fundamental method for the visualization of flow field data and is usually computationally complex and intensive [9]. Feature-based method (e.g., [10] [11]) focuses on regions or coherent structures of a dataset (i.e., features) and exploits the coherence of these regions as they move and interact from one timestep to the next. The method treats regions of interest as independent entities and results in a significant reduction in the storage requirement and rendering cost of visualization tasks, which makes it highly suitable for visualizing the temporal changes of different plumes and WebGL-based exploration so that it is followed in this work.

The visualization of geospatial data (also known as "geovisualization") plays an important role in analyzing and understanding geographic phenomena in earth science. A number of techniques adapted from fields, such as cartography and scientific visualization, are applied to explore geospatial data and through that exploration to generate hypotheses and to develop problem solutions [7]. The methods of geovisualization can be broadly classified into map-based display (or cartographic visualization), animation, visual data mining, and spatio-temporal display [6]. In studying geospatial data with a temporal component such as the sonar image series in this work, animation is often used for efficient displaying the patterns of temporal change with similar properties took place (e.g., the evolution of an earthquake). However, animation needs to compare different portions of data at multiple timesteps which involves memorizing a large number of states in an animated display [6]. This work adopts visual data mining and spatio-temporal display to interactively summarize chosen portions or attributes of the data in selected moments. In geovisualization, visual data mining aims at visually analyzing data and gaining new insights by mapping non-spatial attributes (e.g., weight, accuracy, and risk) of the data

This article has been accepted for publication in a future issue of this journal, but has not been fully edited. Content may change prior to final publication. Citation information: DOI 10.1109/MCG.2020.2995077, IEEE Computer Graphics and Applications

to spatial variables such as length, size, and location. Spatio-temporal display involves a map display to associate the spatial attributes of the data with the temporal attribute. The design of a spatio-temporal display primarily falls into one of the three categories [4]: time-centric design which maps temporal information to one of the spatial dimensions of the display and focuses on the variation of attribute values in the temporal context (e.g., [12]); space-centric design which presents the variation of attribute values in a spatial context and gives a principal attention to the spatial dimensions (e.g., [13]); spatiotemporal design which depicts both spatial and temporal contexts on a display and attempts to give a similar level of attention to both space and time with some abstraction, omission, or distortion (e.g., [14]). In this work, space-centric design and spatiotemporal design are used in the visualizations of plume.

## 3. Acoustic Imaging System and Data

The COVIS instrumentation for the acoustic imaging of plume at hydrothermal vents is designed for use on the deep ocean cabled observatory of NEPTUNE Canada. COVIS is a 4.2-m tall titanium tripod on which the sonar and cable observatory interface systems are mounted (Figure 2a). The sonar images both plumes rising from black smoker vents and the areal distribution of diffuse flow discharging from the surrounding seafloor on a spatial scale of a vent cluster (tens of meters) [15]. COVIS was deployed from Oct 2010 to Oct 2015 at 47°57′N, 129°6′W, approximately 30 m to the north east of the Grotto mound, a hydrothermal vent cluster on the Endeavour Segment of the Juan de Fuca Ridge in the Northeast Pacific, and connected to the junction box and other instruments of the NEPTUNE observatory (Figure 2b). COVIS sits between jumbled blocks of basalt looking south at the north face of Grotto and Dante vent sites (Figure 2c). The sonar scans a plume in 5 minutes during the 2010 deployment and is calibrated to record absolute backscatter intensity. Acoustic images are recorded during 2010 in triplets every 3 hours from a fixed position on the seafloor at a range of 10 to 30 m from several clusters of black smokers on Grotto mound [15]. Video observations show that the largest Grotto plume is produced by coalescence of at least five vents within a 3m × 3m area; in the sonar images, the details of this coalescence are obscured by sidelobe interference by the Grotto edifice. This study focuses on observations of the main buoyant plume and one of two smaller plumes on another part of the Grotto mound; the third plume is not consistently imaged as it often crosses the edges of the ensonified region.

The data used in this paper are a time series of 479 acoustic images (which excludes failed scans due to system malfunction and initial debugging) collected by COVIS over the first 27 days after its installation in September 28, 2010. This dataset can be obtained from the Ocean Networks Canada Data Archive at http://www.oceannetworks.ca. The 3D acoustic images are formed by means of a combination of time gating for resolution in range, digital beam forming for resolution in azimuth, and mechanical scanning for resolution in elevation or height in the plume [16]. Each data frame maps the intensity of the acoustic backscatter from metallic sulfides and temperature fluctuations within the plume onto a 3D grid of 161×121×181 grid points and 0.25-m spacing in all three dimensions. With 1° elevation steps, the azimuthal resolution is 0.5° between half-maximum-power points (and the elevation resolution is 1.0°).

## 4. Design and Approach Overview

### 4.1. Visualization Tasks

The potential audience for the plume visualizations include scientists and students in oceanography. As part of our design process, we interviewed two domain experts and two

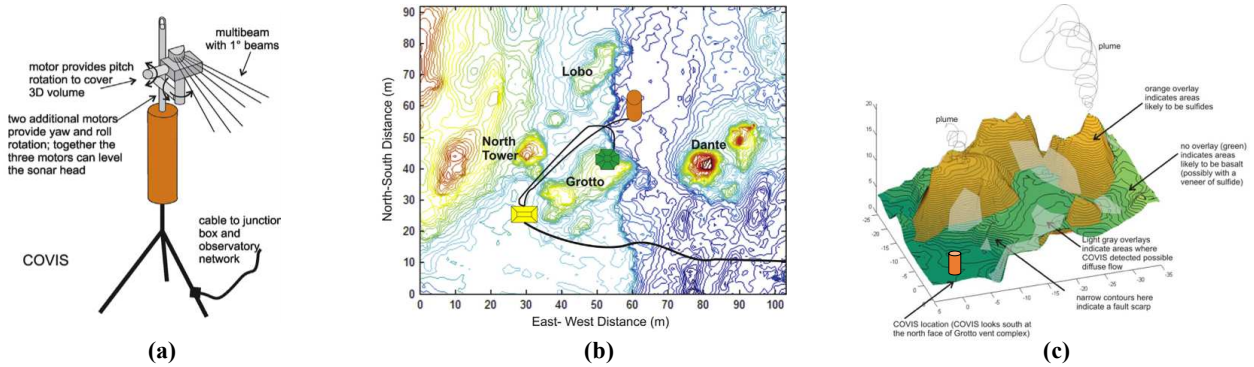


(a) (b) (c)

Figure 2. (a) A schematic diagram of COVIS which fixes a sonar system (acoustic scanning setup) on a tripod and is attached to a junction box on the ocean floor [15]. (b) COVIS (orange cylinder) is deployed just north eastern of Grotto in the Main Endeavour Field on the Juan de Fuca Ridge and is connected to a junction box (yellow box) south of Grotto (yellow trapezoid) as are other instruments sited on the north end of Grotto (green pyramid) [15]. (c) A scenario of two plumes rises up from Grotto which includes two major hydrothermal vents.

This article has been accepted for publication in a future issue of this journal, but has not been fully edited. Content may change prior to final publication. Citation information: DOI 10.1109/MCG.2020.2995077, IEEE Computer Graphics and Applications

graduates to collect their requirements. All of the potential users expect an intuitive and interactive method to facilitate the exploratory visualization of plumes so that they can focus on more advanced questions in research. Based on the requirement analysis, we compiled a list of specific visualization tasks:

***Task 1. Visualize plume objects in the context of ocean floor.*** The system should allow the potential users to visually explore the data in a way that plumes and ocean floor are displayed simultaneously.

***Task 2. Visualize the temporal variations of plume bending and the interaction between the two plumes.*** The system should help viewers observe what timesteps are involved in a cycle, how many cycles a plume goes through in a period of time (say a day), and how the two plumes vary in their bending orientations, sizes, and shapes and interact with each other in a time scale.

***Task 3. Give an overview of the orientation of plume bending.*** The system should present the bending direction and magnitude of plumes in a period of time (e.g., a week) in a concise way.

***Task 4. Summarize the general pattern of plume motion in a dataset.*** The system should provide an insight on what does a plume typically look like in a particular stage of motion and a summary view of a plume in all timesteps of a dataset.

### 4.2. Visual Encodings

In order to fulfill the compiled visualization tasks above, four types of interactive visualizations were proposed and developed: 1. Scenario View, 2. Timeline View, 3. Quadrant View, and 4. Summary View. These visualizations of plumes are well coordinated and allow users to explore hydrothermal plumes from different perspectives.

**a. Scenario View**

This visualization is designed to support exploration of physical entities (Task 1). It adopts a spatial-centric design strategy and overlays both temporal and spatial information of the data on top of spatial dimensions. A Scenario View places the plume objects from one or a bunch of timesteps in the context of the seafloor (bathymetry) to give a reference of the sizes and positions of plumes and illustrates the relationships between the two plumes and the seafloor. The 3D seafloor is generated using the local bathymetry of the ocean basin to create a terrain elevation surface using Delaunay Triangulation. Careful color-coding (both for the plume objects and the seafloor) with visual effectiveness enhancement makes the scenario more real and explainable.

**b. Timeline View**

This visualization is designed for analyzing urban design metrics (Task 2). It adopts the spatiotemporal design strategy and intends to provide visual answers to what timesteps are involved in a cycle, how many cycles a plume goes through in a period of time (say a day), and how the two plumes vary in their bending orientations, sizes, and shapes and interact with each other in a time scale. As shown in Figure 3a, a Timeline View represents each timestep as a unit where the two plume objects in this timestep are placed on the two ends of a rectangular plate and the plume centerlines (scaled to the same length for easy comparison) are put together in the center of the plate. The projections of the centerlines to the horizontal plate are added as direction indicators to remove the possible visual ambiguity in the directions of centerlines. These visual units are connected with each other by a timeline in a way that is similar to a rail.

**c. Quadrant View**

This visualization intends to give an overview of the distribution and variation of plume orientations in a period of time by spatial mapping the bending properties of plumes (non-spatial properties) to a 3D variant of the standard scatter plot (Task 3). In this visualization, an opaque gray plate is plotted on the X-Y plane and is segmented into four quadrants by the X- and Y-Axis which points to the north and east directions respectively (as shown in Figure 3b). The two plume objects in multiple timesteps are placed in either one of the four quadrants based on their azimuths (i.e., quantified bending directions). The distance of a plume object to the coordinate center is decided by either the absolute bending magnitude (the length of projection of the plume centerline in the X-Y plane) or by the relative bending

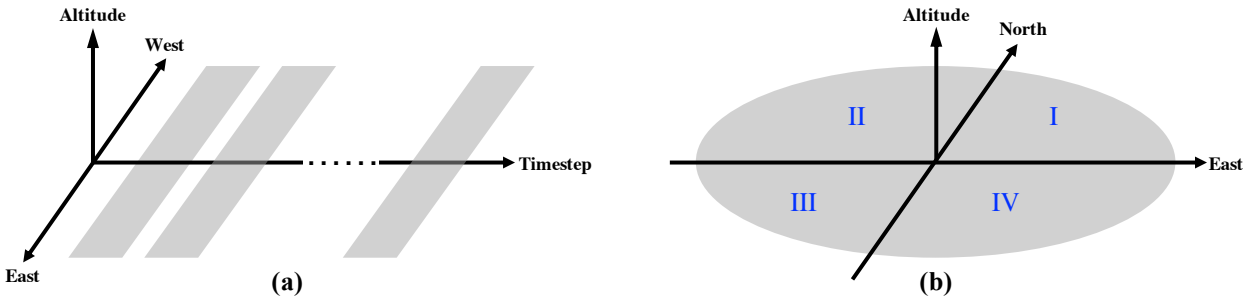


Figure 3. The visualization designs of (a) the Timeline View and (b) the Quadrant View.

This article has been accepted for publication in a future issue of this journal, but has not been fully edited. Content may change prior to final publication. Citation information: DOI 10.1109/MCG.2020.2995077, IEEE Computer Graphics and Applications

magnitude (a ratio of the length of projection to the length of plume centerline). A convex hull is plotted along the boundaries of the plume objects in the visualization.

**d. Summary View**

For a dataset contains hundreds or even thousands of timesteps, the three visualizations that are introduced previously have limitations for summarizing the whole dataset as extremely long timelines or very small images would be needed. A Summary View is aimed to create a set of averages or targeted summaries of plumes across the entire dataset so that the potential users can see a typical view of a plume in a particular stage and a summary in all of the timesteps of the dataset (Task 4). Using the occupancy maps of plume objects, we can create two types of Summary Views: one to give an average visualization for each bending state of a plume; and one to summarize a plume in the entire time series of the data in a single figure. Both types of Summary Views are rendered by direct volume rendering techniques. A common diverging color scheme from ColorBrewer (www.colorbrewer2.org) is adopted to in the visualization to indicate different bending stages of plumes to accomplish visual consistency.

### 4.3. Approach Overview

An overview of the proposed visualization framework is illustrated in Figure 4. The framework is divided into two major parts: data processing and visualization. In the data processing part, time-dependent feature-based algorithms are chosen to generate web-compatible plume metadata. The workflow of the computation starts from extracting plume objects (i.e., features or regions of interest) from every data frame, tracking the extracted plume objects over time, estimating plume centerlines from plume objects, grouping plume objects by their bending orientations, and calculating occupancy maps of plumes in all timesteps of the data. Important geometric properties of plumes are computed in the process. In the visualization part, the four designed visualizations are implemented by combining the WebGL techniques with standard visualization techniques (e.g., surface rendering) so that users can explore the plume metadata from the data processing part in a web browser.

## 5. Data Processing

The approach to data processing combines feature-based time-varying volume visualization with the computation of curve-skeletons and occupancy maps. Investigating plumes as independent objects (i.e., features) highlights their internal properties and individual movements. The availability of the full voxel set for each plume object enables the use of a variety of traditional volume visualization techniques (e.g., isosurfacing and volume rendering) and visual enhancements such as designed colormaps that can depict the occupancy of plumes in an area. The major operations in processing the COVIS data include: identifying and extracting the two major plumes from each data frame in the time series of data; matching the extracted plume objects from a timestep to the next over a pre-specified time range to build their correspondences; finding the centerline of each plume object and further computing some geometric properties (e.g., altitude and azimuth); defining a plume bending model to classify plume objects into five bending states by their bending orientations; and calculating occupancy maps to reflect the occurrences of plumes in each voxel of the data frame over all timesteps.

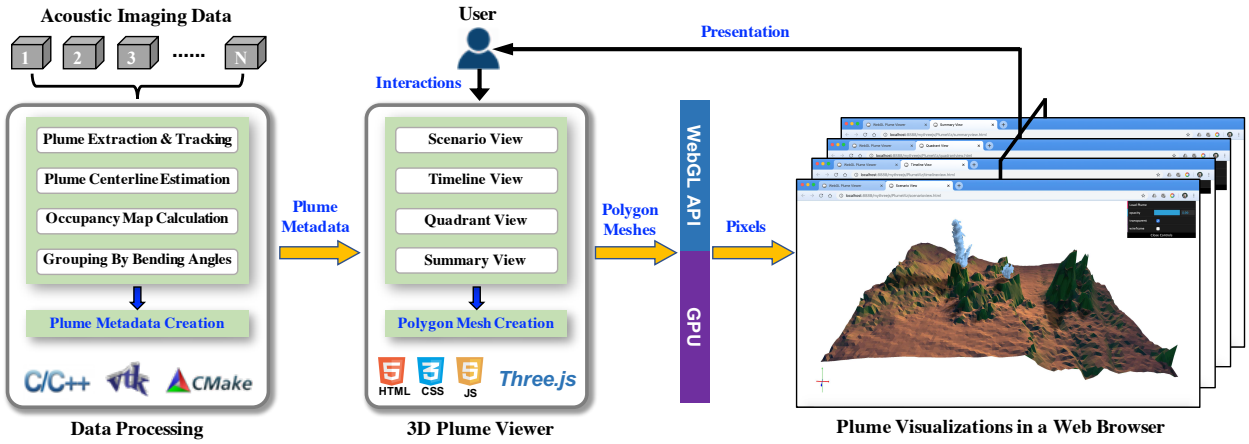


Figure 4. An overview of the proposed plume visualization framework. The framework includes a data processing part and a 3D plume viewer: the data processing algorithm generates web-compatible metadata for visualization; the 3D plume viewer reads and converts the metadata to a series of polygon meshes and renders the polygon meshes as visualizations in a web browser using the WebGL API and the capabilities of GPUs. Users' interactions with the graphic user interface and the visualizations are supported in the viewer.

This article has been accepted for publication in a future issue of this journal, but has not been fully edited. Content may change prior to final publication. Citation information: DOI 10.1109/MCG.2020.2995077, IEEE Computer Graphics and Applications

### 5.1. Plume Object Extraction and Tracking

The first step isolates the hydrothermal plumes from the background of each data frame (i.e., timestep). In the visualization literature, this is variably referred to as segmentation or extraction. Plumes are isolated from the background region (defined as voxels with values less than a predefined threshold) as independent objects by applying a three-dimensional region-growing algorithm to the gridded data. The region-growing algorithm starts with a single seed node (usually location of the maximum value) and recursively searches all adjacent voxels to the chosen seed point; those with intensity greater than the threshold are labeled as belonging to the current feature. All searched voxels are marked as visited. The current feature stops growing when only voxels with values less than the threshold are encountered in all growing directions. The algorithm then repeats, choosing an unvisited voxel with intensity greater than the predefined threshold as a new seed point. Each seed point is assigned a unique object ID. The set of voxels that constitute the plume object (i.e., the grown region) are stored in a data structure for efficient manipulation. The region-growing process is completed when all voxels in the data are visited. Spatial properties of each extracted object, such as volume, centroid, and bounding box, etc. are calculated for each resulting plume object. To reduce the rendering cost for an efficient visualization, the Marching Cubes algorithm [17] is applied to compute an isosurface of each plume object. Using isosurfaces, a volume object can be rendered by a simple polygonal. The algorithm saves the data points and isosurface for each plume object separately as the metadata for visualization.

Tracking is used to determine the occurrences of the same plume over the consecutive timesteps. It forms the basis of observing the temporal variation of plumes in a time series. The extracted plume objects in each timestep are correlated over time with a feature-tracking algorithm based on volume overlap [11]. After tracking, a correspondence list (tracking history) is created to record the evolution of features in every timestep.

### 5.2. Plume Centerline Estimation

The centerline of a plume is the geometric axis of a plume and is a reference for the radial distribution of plume properties, the interaction between plumes, and the orientation of a plume in space. A centerline can be used to accurately estimate plume properties such as the bending orientation, peak intensity (based on the overall distribution), the peak location, and the e-folding radius of the plume. Several advancements have been made in centerline and plume property computations. In many early (and some current) applications, centerlines were defined using a series of horizontal slices at varying heights above the vent. A more advanced (and accurate) method first computes a curve-skeleton of a plume object [18] then fit a centerline from the computed plume skeleton. In this work, we adopted a curve-skeleton algorithm that is using a distance field. As a flowchart shown in Figure 5, the process of centerline computation includes five steps: (1) classifying all voxels in a plume object into boundary and interior voxels and assign each voxel a tag; (2) computing the distance between each interior voxel and the nearest boundary voxels and generating a distance field for each plume object; (3) finding the local maxima (ridge points) in the computed distance fields; (4) connecting ridge points to form the plume centerline; and (5) least-squared estimating and fitting a centerline from the computed plume skeleton.

Geometric properties of plumes including radius, length, connectivity of constituent objects, and bending orientation are computed to provide a basis of quantitatively comparing the behavior of different hydrothermal plumes [19] and to assess entrainment and expansion rates, especially as they relate to interaction between plumes and with the surrounding environment [3].

### 5.3. Grouping Plume by Bending Orientations

This step categorizes plume objects by their bending orientations. Theoretically, tidal currents push a plume in directions that vary in an elongated ellipse such that the primary motion appears as sloshing back-and-forth along the long axis of the ellipse as illustrated in Figure 6a (or,

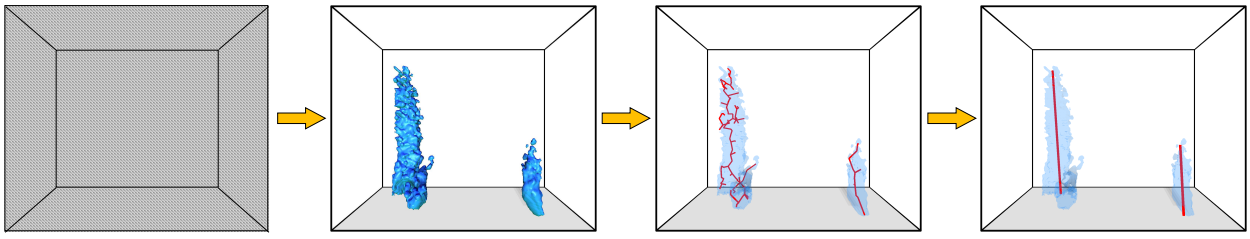


Figure 5. The process of finding centerlines of plumes in a chosen timestep. (a) The two plume objects are extracted from the background of the chosen data frame. (b) Curve skeletons of each plume object are computed to keep the topology of plumes. (c) Plume centerlines are determined as the least squares fits to the plume skeletons.

This article has been accepted for publication in a future issue of this journal, but has not been fully edited. Content may change prior to final publication. Citation information: DOI 10.1109/MCG.2020.2995077, IEEE Computer Graphics and Applications

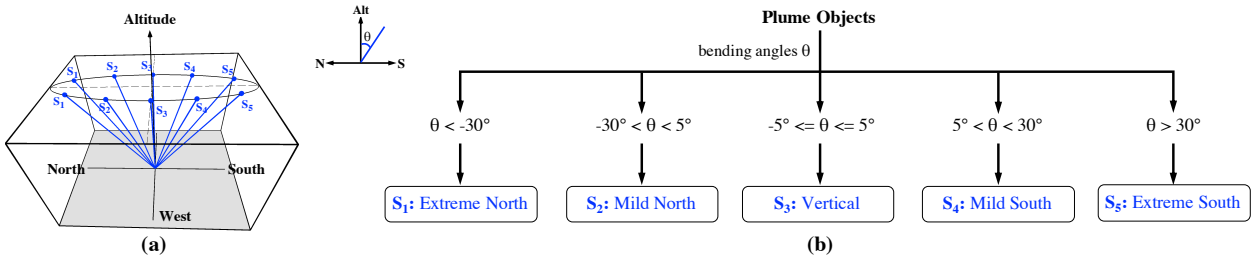


Figure 6. (a) The idealized elliptical rotation of tidal currents that drives a plume to move along an elliptical path. (b) A plume bending model is designed for grouping plumes into either one of the five bending states by the bending angles of the plumes.

geologically, along the axis of the rift valley [15]). Although the true motion is elliptical, the direction of bending for near-vertical (<5° from vertical) plumes is not robust against minor errors (<2 m) in the location of ridge points; thus the idealized model in Figure 1 simplifies the elliptical bending into planar bending. Furthermore, the rift valley on the Juan de Fuca Ridge is oriented roughly north-south (about 20°NE to SW). Inspired by the five idealized and hypothesized plume bending classifications in Figure 1, we design a plume bending model to classify the elliptical bending motion of a plume into five bending states within an assumed vertical plane along the long axis of the ellipse: S1: extreme bending to the north; S2: mild bending to the north; S3: little to no bending; S4: mild bending to the south; and S5: extreme bending to the north. We took the advice from the domain experts and assigned the following conditions for each bending state in the model: "θ < -30°" for S1; "-30° < θ < -5°" for S2, "-5° <= θ <= 5°" for S3; "5° < θ < 30°" for S4; and "θ > 30°" for S5, where θ is the degree of bending relative to vertical. The designed plume bending model is illustrated in Figure 6b. Using the plume bending angles previously estimated using least-squares fitting of the connected ridge points, each of the two plumes in each timestep across the whole dataset are grouped into one of the five bending states by implementing the classification algorithm of the model.

### 5.4. Occupancy Map Calculation

By grouping all of the instances wherein a plume object passes through a defined bending state (S1 – S5), we can actually get an "average view" of the plume at that state and even go a step further to ask for a summary picture of the entire database of events. Using the computed plume objects and their bending orientations, a new set of averages or targeted summaries are built around the concept of occupancy map. In this work, we create two types of occupancy map to summarize the general pattern of the plume bending across the dataset.

The first type of occupancy map counts the occupation frequency of a plume object over all of the timesteps at every voxel of the data frame and uses these computed frequencies as voxel values. The occupation frequency or the voxel value at the location (i, j, k) can be calculated as follows:

$$O(i,j,k) = \sum_{t=1}^{t=N} V(t)_{i,j,k}$$

where N is the number of timestep in the dataset (i.e., 479 in this work). V(t) equals to 1 if the plume object occupies the voxel (i, j, k) at the timestep t or 0 otherwise.

The second type of occupancy map counts different occupation frequencies of the plume object in different bending states (S1 – S5) at every voxel and assigns a voxel value from 1 to 5 based on the dominant bending state.

## 6. Usage Scenarios

We developed PlumeViz, a WebGL-based plume viewer for presenting the developed visualizations within web browsers. Written in JavaScript language with the support of Three.js library (https://github/mrdoob/three.js), the viewer supports interactive surface and volume rendering of plume objects (metadata of the data processing) and underlying 3D geographic maps through the WebGL API and the capabilities of GPU in computers. As a browser-running visualization tool, PlumeViz has the benefit of not requiring a client-side installation, offering centralized maintenance, and ensuring a common environment for all users, which promotes collaborative research and customized extensions. In the rest of this section, we present two usage scenarios conducted with the PlumeViz.

### 6.1. Scenario One: Studying Plume Motion in A Period of Time

In the first scenario, scientist A was doing a daily analysis of plume motion. She would like to: (a) explore the plumes from a set of timesteps; (b) observe how the two plumes vary in their bending orientations, sizes, and shapes and interact with each other in a time scale; and (c) understand the general distribution of plume orientations.

The scientist first opened the webpage "Scenario View" from the user interface of PlumeViz and selected a timestep of isosurface metadata for visualization. In Figure 7a, the

This article has been accepted for publication in a future issue of this journal, but has not been fully edited. Content may change prior to final publication. Citation information: DOI 10.1109/MCG.2020.2995077, IEEE Computer Graphics and Applications

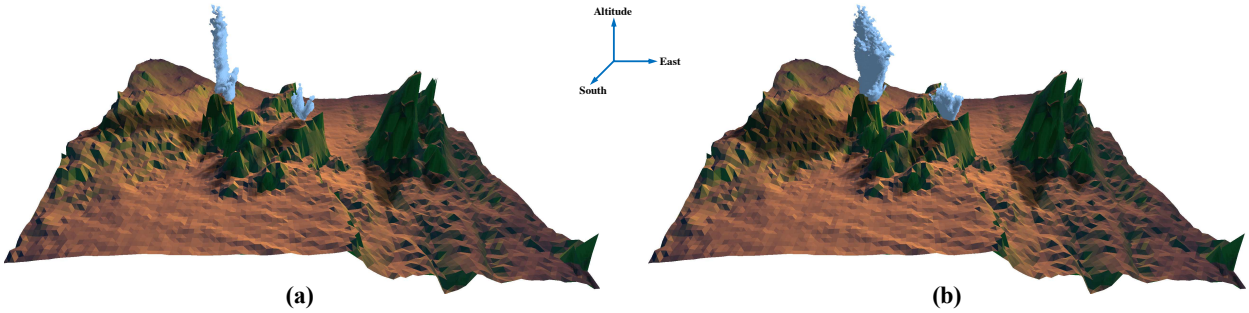


Figure 7. Two Scenario Views showcase plumes rose from hydrothermal vents on the seafloor. (a) The plume objects in the 93rd timestep (3:00 AM, October 9, 2010). (b) The plume objects from all 24 timesteps of the day October 9, 2010.

Scenario View showcases the scenario where the two major plumes in the selected timestep (3:00 AM, October 9, 2010) rose from the Grotto vents. The scientist then selected all of the 24 timesteps on October 9, 2010 and visualized the combination of plumes in the same context (Figure 7b). As seen in Figure 7, the large plume (located in the west) has a form similar to a pillar while the small plume (located in the east) has a bifurcate shape.

After having some basic ideas about the shape, size, and position about the plumes for study, the scientist opened the webpage "Timeline View" from the user interface and started to observe the temporal properties of plumes in different days. In Figure 8, the plumes in all timesteps of two chosen days (October 1, 2010 and October 8, 2010) are presented as two Timeline Views. The visualization on the top (October 1) suggests a strong semi-diurnal periodicity (2 cycles/day) for the bending motions of both the large plume (cycle1: 1 – 8 timesteps; cycle2: 9 – 24 timesteps) and the small plume (cycle1: 1 – 10 timesteps; cycle2: 11 – 24 timesteps), which is consistent with the hypothesis that plume motion is periodic at tidal frequencies and is also observed in spectral analyses of the bending direction and amplitude and of vertical velocity estimates from related data [20]. In contrast, the semi-diurnal periodicity is less pronounced in the visualization on the bottom (October 8) which displays only one cycle a day for both the large and small plumes. Besides the bending periodicity, the Timeline Views suggest the primary motion of plume is sloshing back-and-forth along the north-south direction (i.e., the long axis of the ellipse in Figure 6a). The scientist also found that the centerline of the small plume always tends to bend towards the large plume. This bending tendency suggest the interaction between the two plumes can probably be simplified as the entrainment field of the large plume.

Finally, the scientist opened the webpage "Quadrant View" to analyze the distribution of plume orientations. As

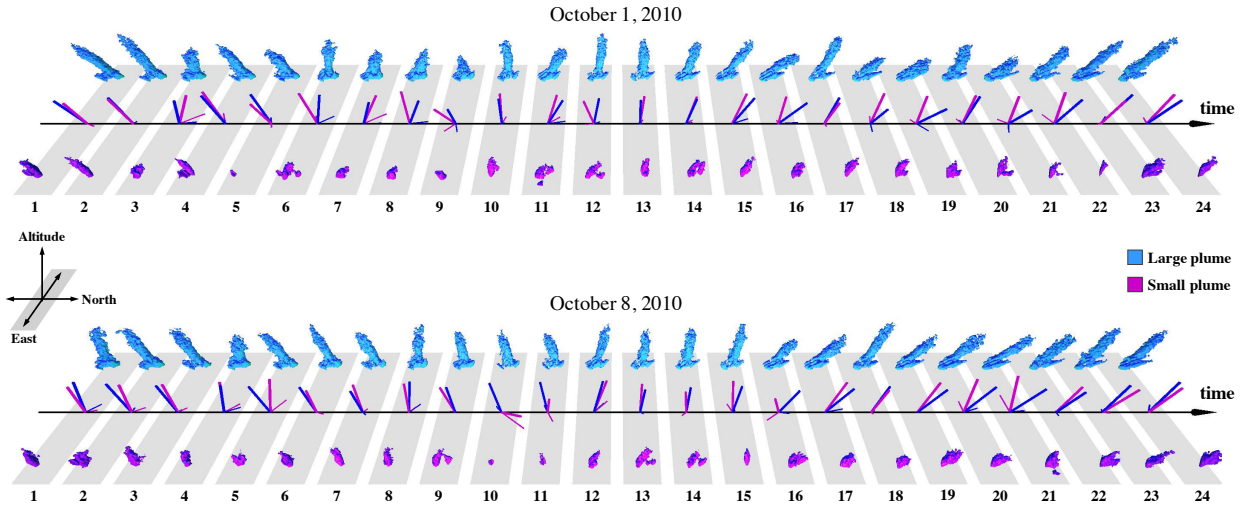


Figure 8. The plume bending motions of two chosen days are presented as two Timeline Views (top: October 1, 2010; bottom: October 8, 2010). The plumes objects along the timeline showcase the temporal variation of the height, radius, shape, and bending direction in the motion. The two plume centerlines (scaled to the same length) are placed together to compare the bending motions of and to observe the interactions between the large and small plumes.

This article has been accepted for publication in a future issue of this journal, but has not been fully edited. Content may change prior to final publication. Citation information: DOI 10.1109/MCG.2020.2995077, IEEE Computer Graphics and Applications

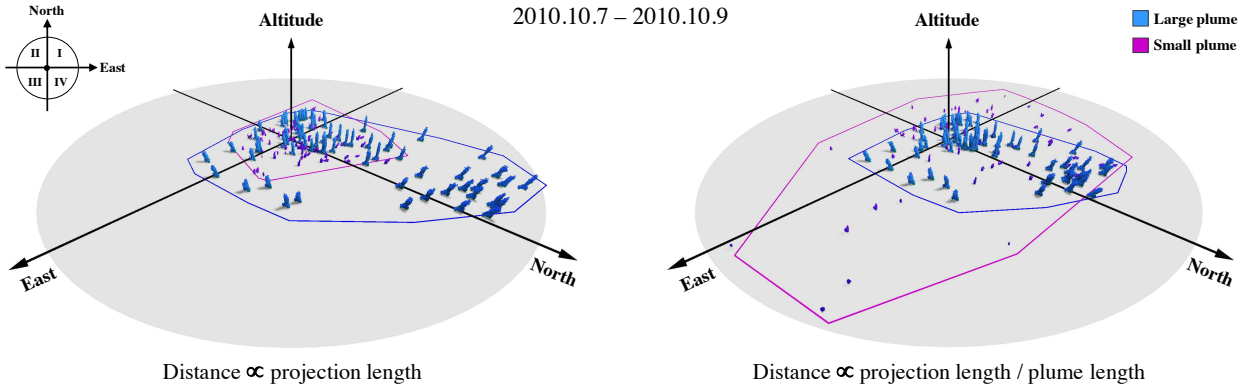


Figure 9. The Quadrant Views present plumes in all timesteps of three chosen days (October 7 – 9, 2010). The plume objects (blue for the large and pink for the small) are placed in four quadrants based on their azimuths (quantitative bending directions). The distance of a plume object to the coordinate center is decided by either the absolute bending magnitude (left panel) or by the relative bending magnitude (right panel).

shown in Figure 9, the plume objects in all timesteps of three chosen days (October 7 – 9, 2010) are presented as two Quadrant Views. By comparing the areas of the two plume distribution boundaries in Figure 9a and 9b, she noticed that the large plume has a bigger absolute bending magnitude and smaller relative bending magnitude than the small plume. Moreover, both plume objects gather in the second quadrant more frequently than they do in the other three quadrants, which implies the direction of the joint force from oceanic and geological external forcing fields is northwest-ward during this time period.

### 6.2. Scenario Two: Summarizing A Plume Object in The Dataset

In the second scenario, scientist B was doing a longitudinal study of plumes. Considering the large number of timesteps that would be involved, he believed that studying the motion and variation of a plume by timesteps or days was no longer effective. Instead, he would like to see an average view of a plume in a particular stage and further see a summary of a plume in all of the timesteps in the dataset.

The scientist opened the webpage "Summary View" from the user interface and selected all timesteps of data point metadata for visualization. In Figure 10a, five "first-type" occupancy maps (the voxel value equals to the occupation frequency at this voxel) of the large plume are volume-rendered with the frequency of plume occurrence in each voxel color-coded by a diverging colormap in which the color varies from cold to hot as the frequency increases. As can be found from the figure, these "averaged plumes" of the five bending states (S1 - S5) reveal a clear asymmetry of the plume bending response and thus the driving force of tidal currents: the plume bends much more strongly to the north (S1 and S2) than to the south (S4 and S5). The scientist also found that the plume gets thicker (or has a bigger radius) as it bends to the two extremes and it remains the thinnest in the vertical state (S3). In Figure 10b, the "second-type" occupancy map (the voxel value equals to a bending state) of the large plume is volume rendered with five unique colors to indicate the occupancy of the five bending states. The front view of the visualization shows that the areal extent across the vertical plane of bending derives from the systematic bending response to ocean currents. From the side view and top view, the scientist B drew a conclusion that the bending motion of the plume is not in an ideal plane as the plume model in the laboratory predicts [1] [3]. The incidences of plume at each bending state, which is reported in the bar chart on the left of Figure 10b, also shows the asymmetry of plume bending.

## 7. Science Learned

In this section, we discuss the scientific findings arose from the plume visualizations. These findings summarize the actual plume behaviors from the acoustic imaging of hydrothermal plume used in this work and thus are valuable to understand the complex temporal behavior of hydrothermal plumes.

***The primary motion of a plume appears as sloshing back and forth on a nearly elliptical track.*** From Figure 9 and 10b, it is easy to find that the bending motion of a plume is not in an ideal plane but closer to an ellipse as the plume model in the laboratory predicts [1] [3]. In Figure 10b, at the extremes of bending in the state S1 (pink) and the state S5 (dark blue), the plume leans out of the plane of bending defined by the inner stages (states S2 – S4). This out-of-plane bending could be induced by ocean currents and reflects the complexity of the ocean currents. The Timeline Views in Figure 8 suggest the bending magnitude along the north-south direction is much larger than that along the east-west direction. Ideally, the back-and-forth sloshing of a

This article has been accepted for publication in a future issue of this journal, but has not been fully edited. Content may change prior to final publication. Citation information: DOI 10.1109/MCG.2020.2995077, IEEE Computer Graphics and Applications

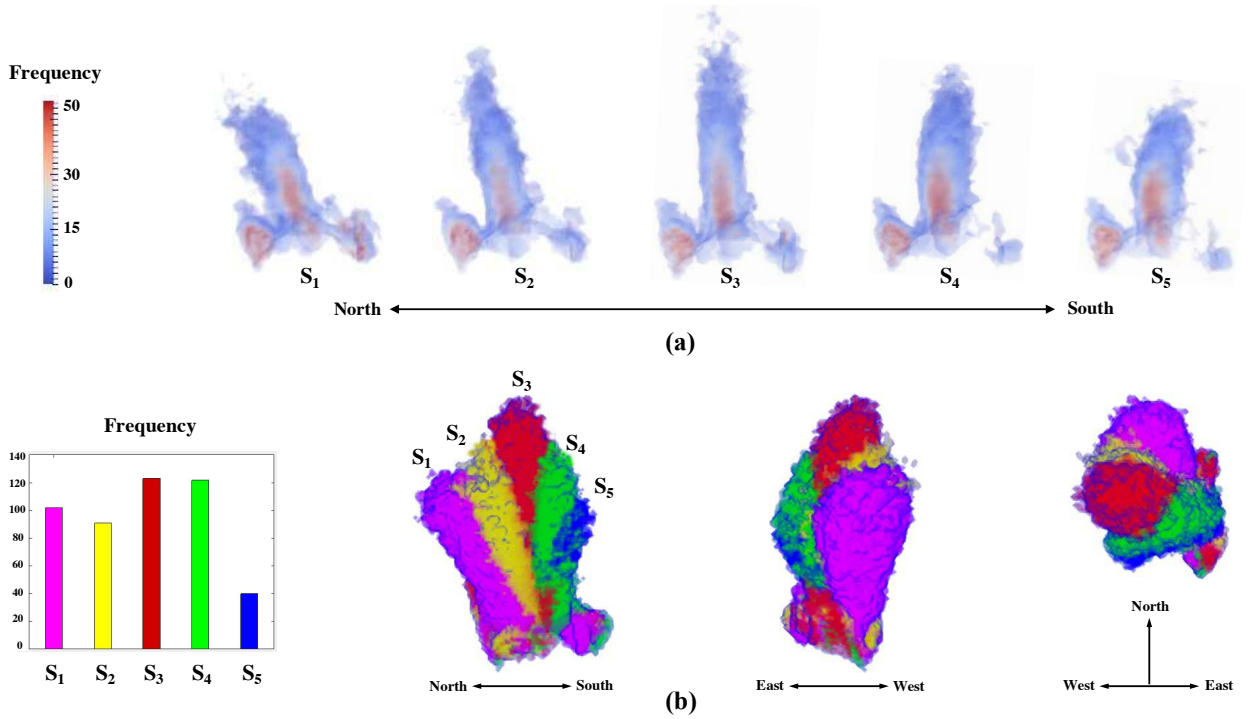


Figure 10. (a) This Summary View shows five "average plumes" for the five bending states. Each "average plume" summarizes all of the instances of the large plume in a given bending state. A diverging colormap is used to indicate the frequency of plume occurrence in each voxel. (b) This Summary View summarizes the bending motion of the large plume across the whole dataset. On the left, the incidences of the plume in the five bending states are given in a bar chart. On the right, the visualization is presented in front view, side view, and top view. Each voxel in the occupancy map is colored by a distinct color that represents a bending state.

plume is along the long axis of an ellipse (as illustrated in Figure 6a) or the axis of the rift valley geologically [15].

***The plumes generally bend with periodicities similar to the semi-diurnal tidal cycle with some aperiodic or complex patterns of bending in the process.*** As noted in the introduction, ocean currents include both ocean tides, which induce a periodic change in the direction and magnitude of the orientation of plumes, and occasional storm-driven (or otherwise produced) internal waves, which disrupt the normal ocean tidal currents resulting in aperiodic patterns of bending. In Figure 8, the Timeline View on the top suggests a strong semi-diurnal periodicity (2 cycles/day) for the bending motions of both the large and the small plumes, which is consistent with the hypothesis about the periodicity of plume motion and was confirmed by spectral analysis of the bending direction and amplitude. However, the Timeline View on the bottom only displays one cycle for both plumes, which implies interference by internal waves was dominant during that day.

***The entrainment by a larger (stronger) plume modifies the response of smaller plume(s) to the ocean tidal currents.*** In Figure 8, the centerline of the small plume always tends to bend towards the large plume. This bending tendency suggests that the entrainment field of the large plume is much stronger than that of the small plume and that the entrainment by the large plume modifies the response of the small plume to the ocean tidal currents. The different distributions of plume objects in the Quadrant Views (Figure 9) indicate that the large plume has a bigger absolute bending magnitude (left) and smaller relative bending magnitude than the small plume (right). In other words, the small plume is more strongly affected by currents (higher normalized motion). However, because a shorter height is displayed for a given isovalue, the absolute bending motion is smaller. More broadly, we can draw the conclusion that the interaction effect between the two plumes can be simplified as the entrainment field of the large plume.

***The entrainment rate of a plume is positively correlated with the bending angle of the plume.*** As can be found from Figure 10, the "average" of the large plume gets thicker as it bends from the center to the two sides and it remains the thinnest in the vertical state (S3). This visual increase of the radius (i.e., the thickness) with plume bending confirms the hypothesis that entrainment increases with the speed of tidal currents impinging on the plume edge, which is called forced entrainment.

***Plume bending indicates the asymmetry of local currents.*** As shown in Figure 9, plume objects gather in the

second quadrant more often than they do in the other three quadrants. This tendency in the distribution of plume bending is consistent with a mean flow north-westwards in the rift valley during this time period with episodic excursions in other directions that may relate to storm-generated internal ocean waves [15]. In Figure 10, the Summary View reveals a clear asymmetry of the plume bending response and thus the driving force of tidal currents: the plume bends much more strongly to the north than to the south. This asymmetry is consistent with other observations of a mean northward flow in parts of the Endeavour Segment rift valley [15]. Furthermore, although the state S5 appears similar to S4, the slight shortness of S5 indicates that much of the bending in S5 is out of the typical plane defined by tidal currents.

## 8. Conclusion and Future Development

Visualizing hydrothermal plumes helps develop scientific insight into volcanic activities on the seafloor. The motivation of this work is to use data visualization techniques to facilitate the visual exploration and quantitative analysis of hydrothermal plumes and to help domain scientists compare the actual behavior of plumes with that predicted by tidal interaction models and buoyant plume models incorporating forced entrainment effects. Inspired by the hand-drawn figurative depiction of hydrothermal plumes (e.g., Figure 1), this work combines the methods of geovisualization with time-varying feature-based data processing to create four types of visualizations of plumes from acoustic imaging of hydrothermal plumes collected from the COVIS in the Northeast Pacific. The visualization results effectively demonstrate the basic properties of hydrothermal plumes and the linkages of the elliptical plume motion with oceanic and geological external forcing fields. Moreover, the visualizations established that hydrothermal plumes are structured similar to the model plumes in laboratories.

Given this initial success, we intend to extend the capabilities of the proposed visualizations. First of all, we plan to explore more types of visualization to summarize the data and to couple different visualizations in the viewer (i.e., PlumeViz) more tightly with each other. Secondly, we have only applied the proposed visualizations to COVIS data in this work. Exploring other datasets or different acoustic images from the same dataset with the visualizations is on our plan. Last but not least, we intend to process data from the simulation environment or other powerful centralized infrastructure instead of downloading and processing the data locally. This client-server architecture will leave the heavy computation tasks in the server-side so that the client-side can execute as few operations as possible to obtain a directly renderable representation.

## ACKNOWLEDGEMENT

We thank Ocean Networks Canada and the Department of Marine and Coastal Sciences at Rutgers University for facilitating the acquisition of the acoustic images of hydrothermal plume and the domain experts who gave us feedback to this project. This work has been funded by US National Science Foundation (NSF) Grants OCE-1234141.

## APPENDIX: Computer Code and Data

The computer code in this manuscript includes a standalone C/C++ program for data processing and the PlumeViz, a WebGL-based viewer for hydrothermal plumes. Any questions regarding the computer code, please contact the developer and the author Li Liu: lliu6819@suda.edu.cn

### - Data Processing Program

This program reads a series of COVIS data frame and creates a set of metadata (e.g., *.poly files, *.uocd files, *.skl files etc.) for visual exploration and data analysis. More information about the program, the accesses to the source code and data, and how to run the code can be found at: http://vizlab.rutgers.edu/covis_processing

### - PlumeViz

PlumeViz is a WebGL viewer which takes the metadata of plumes (*. poly and *. uocd files) as input and presents the visualizations in web browsers. The introduction of and the access to the viewer and a testing dataset can be found at: http://vizlab.rutgers.edu/plume_viewer

### - COVIS Data

The COVIS data can be accessed from the Ocean Networks Canada Data Archive at http://www.oceannetworks.ca. Any questions regarding the data, please contact Dr. Karen Bemis: bemis@marine.rutgers.edu

## Reference

[1] Di Iorio, Daniela, J. William Lavelle, Peter A. Rona, Karen Bemis, Guangyu Xu, Leonid N. Germanovich, Robert P. Lowell, and Gence Genc. "Measurements and models of heat flux and plumes from hydrothermal discharges near the deep seafloor." Oceanography 25, no. 1 (2012): 168-179.

[2] German, Christopher R., K. A. Casciotti, J-C. Dutay, Lars-Eric Heimbürger, William J. Jenkins, C. I. Measures, R. A. Mills et al. "Hydrothermal impacts on trace element and isotope ocean biogeochemistry." Philosophical Transactions of the Royal Society A: Mathematical, Physical and Engineering Sciences 374, no. 2081 (2016): 20160035.

[3] Rona, Peter A., Karen G. Bemis, Christopher D. Jones, Darrell R. Jackson, Kyohiko Mitsuzawa, and Deborah Silver. "Entrainment and bending in a major hydrothermal plume, Main Endeavour Field, Juan de Fuca Ridge." Geophysical research letters 33, no. 19 (2006).

[4] Abdul-Rahman, Alfie, Simon Walton, Karen Bemis, Julie Gonnering Lein, Katharine Coles, Deborah Silver, and Min Chen. "Re-spatialization of time series plots." Information Visualization 16, no. 4 (2017): 275-290.

[5] Thomson, Richard E., Marina M. Subbotina, and Mikhail V. Anisimov. "Numerical simulation of mean currents and water property anomalies at Endeavour Ridge: Hydrothermal versus topographic forcing." Journal of Geophysical Research: Oceans 114, no. C9 (2009).

[6] Nöllenburg, Martin. "Geographic visualization." Human-centered visualization environments. Springer, Berlin, Heidelberg, 2007. 257-294.

[7] Kraak, Menno-Jan. "Geovisualization illustrated." ISPRS journal of photogrammetry and remote sensing 57, no. 5-6 (2003): 390-399.

[8] Ma, Kwan-Liu. "Visualizing time-varying volume data." Computing in Science & Engineering 5, no. 2 (2003): 34.

[9] Zhang, Jiang, and Xiaoru Yuan. "A survey of parallel particle tracing algorithms in flow visualization." Journal of Visualization 21, no. 3 (2018): 351-368.

[10] Samtaney, Ravi, Deborah Silver, Norman Zabusky, and Jim Cao. "Visualizing features and tracking their evolution." Computer 27, no. 7 (1994): 20-27.

[11] Silver, Deborah, and Xin Wang. "Tracking and visualizing turbulent 3d features." IEEE Transactions on Visualization and Computer Graphics 3, no. 2 (1997): 129-141.

[12] Lu, Aidong, Wei Chen, William Ribarsky, and David Ebert. "Year-long time-varying 3D air quality data visualization." In Advances in Information and Intelligent Systems, pp. 289-306. Springer, Berlin, Heidelberg, 2009.

[13] Liu, Li, Deborah Silver, Karen Bemis, Dujuan Kang, and Enrique Curchitser, "Illustrative visualization of mesoscale ocean eddies." Computer Graphics Forum, vol. 36, no. 3, pp. 447-458, 2017.

[14] Andrienko, Natalia, and Gennady Andrienko. "Interactive visual tools to explore spatio-temporal variation." In Proceedings of the working conference on Advanced visual interfaces, pp. 417-420. ACM, 2004.

[15] Bemis, Karen G., Deborah Silver, Guangyu Xu, Russ Light, Darrell Jackson, Christopher Jones, Sedat Ozer, and Li Liu. "The path to COVIS: A review of acoustic imaging of hydrothermal flow regimes." Deep Sea Research Part II: Topical Studies in Oceanography 121 (2015): 159-176.

[16] Light, R., V. Miller, P. Rona, and K. Bemis. "Acoustic instrumentation for imaging and quantifying hydrothermal flow in the NEPTUNE Canada Regional Cabled Observatory at Main Endeavour Field." (2012).

[17] Lorensen, William E., and Harvey E. Cline. "Marching cubes: A high resolution 3D surface construction algorithm." In ACM siggraph computer graphics, vol. 21, no. 4, pp. 163-169. ACM, 1987.

[18] Cornea, Nicu D., Deborah Silver, and Patrick Min. "Curve-skeleton properties, applications, and algorithms." IEEE Transactions on Visualization & Computer Graphics 3 (2007): 530-548.

[19] Rona, P. A., K. G. Bemis, D. Silver, and C. D. Jones. "Acoustic imaging, visualization, and quantification of buoyant hydrothermal plumes in the ocean." Marine Geophysical Researches 23, no. 2 (2002): 147-168.

[20] Xu, G., D. R. Jackson, K. G. Bemis, and P. A. Rona. "Observations of the volume flux of a seafloor hydrothermal plume using an acoustic imaging sonar." Geochemistry, Geophysics, Geosystems 14, no. 7 (2013): 2369-2382.

## Bios

Li Liu is an associate professor in the School of Computer Science and Technology at Soochow University, China. His research focuses on machine learning and data visualization. He received his Ph.D. from Rutgers University in Computer Engineering.

Deborah Silver is a professor in the Department of Electrical and Computer Engineering at Rutgers University. Her research interests include data visualization and computer graphics. She received her Ph.D. from Princeton University in Computer Science.

Karen Bemis is an assistant research professor at Rutgers University. Her research interests include exploring uses of scientific visualization in geologic problems and the psychology of understanding and using visualizations. She received her Ph.D. from Rutgers University in Geological Sciences.